

TAXONOMY AND CLASSIFICATION SCHEME FOR ARTIFICIAL SPACE OBJECTS

C. Früh⁽¹⁾, M. Jah⁽²⁾, E. Valdez⁽³⁾, P. Kervin⁽⁴⁾, and T. Kelecý⁽⁵⁾

⁽¹⁾*Mechanical Engineering Department, University of New Mexico / Air Force Research Laboratory, Space Vehicles Directorate, NM 87117, USA*

⁽²⁾*Air Force Research Laboratory, Space Vehicles Directorate, Albuquerque, NM 87117, USA*

⁽³⁾*United States Geological Survey, Dept. of Biology, University of New Mexico, NM 87117, USA*

⁽⁴⁾*Air Force Maui Optical & Supercomputing (AMOS), Kihei, HI, 96753, USA*

⁽⁵⁾*The Boeing Company, Colorado Springs, CO, 80919, USA, Email: thomas.m.kelecý@boeing.com*

ABSTRACT

As space gets more and more populated, a classification scheme based upon scientific taxonomy is needed to properly identify, group, and discriminate space objects. Using artificial space object taxonomy also allows for scientific understanding of the nature of the space object population and the processes, natural or not, that drive changes of an artificial space object class from one to another.

In a first step, an ancestral-dynamic hierarchical tree based on a priori knowledge is established, motivated by taxonomy schemes used in biology. In a second step, available orbital element data has been clustered. Therefore, a normalization of a reduced orbital element space has been established to provide a weighting of the input values. The clustering in the five dimensional normalized parameter space is divided in two sub-steps. In a first sub-step, a pre-clustering in a modified cluster-feature tree has been applied, to initially group the objects and reduce the sheer number of single entities, which need to be clustered. In a second sub-step, a Euclidean minimal tree algorithm has been applied, to determine arbitrarily shaped clusters. The clusters also allow determination of a passive hazard value for the single clusters, making use of their closest neighbors in the minimal tree and the radar cross section of the cluster in question.

Key words: taxonomy; classification; space debris.

1. INTRODUCTION

A study of a set of different objects leads to a specific set of parameters describing the characteristics of those objects. With the increasing number of objects and accuracy to capture all possible characteristics, a large parameter space is utilized. In order to make the data set accessible and manageable, it is desired to reduce

the parameter space to significant quantities which allow determination of differences and similarities between different objects and to group and classify them accordingly. However, the aim is not to introduce a random grouping, but to find a taxonomy of significant parameters corresponding to an actual physical and behavioral (e.g. dynamic) attributes.

Currently, about 20,000 objects are cataloged in the publicly available USSTRATCOM catalog, whereas in situ measurements suggest around 300,000 objects to be in orbit around the Earth. So far, only a very broad taxonomy has been applied in different orbital regions, such as the orbital classifications of geostationary, geostationary transfer orbits, Molniya, low Earth orbits, which have been applied ad hoc. Another classification scheme is based subsets of objects, such as the ESA Classification of Geosynchronous objects, sorting objects by their orbital evolution, such as objects in drift orbits, around libration points, or controlled orbits. Another classification that has been readily adopted is the discrimination in classified and unclassified objects. If in the following the term classification is used, it prescribes the scientific terminology and shall not be confused with a security relevant grouping of objects. But discussions are ongoing about that a refinement of this structure is needed. In the following, only unclassified objects are taken into account. In this paper the focus is on orbital element classification. The important topic of further means of characterization and classification based on the inclusion of spectral and light curve measurements is not discussed here.

The oldest taxonomic systems are rooted in biology primarily established by Aristotle. Biological taxonomy orders plants and animals into an organized system that includes species, genera, families and higher forms of taxonomy. The system as applied to biology also shows that taxonomies are not static, but subject to change over time as new knowledge arises. Mayr defines the crucial steps [11] in building a taxonomy of any kind: The first step is (1) the *collection* of possible data, as a second step he defines (2) the *identification*. At the

identification step the individual objects are sorted in groups. The challenge is to select the relevant groups, which are as broad as possible, while not overlooking distinguishing features; the identification is, in general, the analytical taxonomy step. The identification also includes the process of naming the groups that have been identified with a useful term that is precise enough to represent the group, but also short enough to be useful. As a third step, (3) the *classification* follows as a synthetic taxonomy categorization. In this step the different identified genera and species are ordered. Available a priori knowledge can be fed in, in addition to assessing the physical reality of the defined classes. The aim is to find an ancestral descent of the different genera and species, and their interrelations. Using traditional morphological taxonomy, convergence to a habitual state is sought, e.g.. As it is easily conceived, the three steps are highly interdependent. The data at hand determines and limits the identification that is actually possible, and identification is reiterated depending on the classification step. As new knowledge independent of the initial data set is added, classification can change, which traces back to the identification step. This complete interdependent system of data, identification and classification is named the taxonomy.

The taxonomic classification used in astronomy has the most overlap with the problem of artificial space objects are perhaps asteroids. Taxonomy systems of asteroids are traditionally based on color measurements (filter UVB and spectroscopic measurements) and albedo (including polarimetry). Earliest classifications of asteroids [17] were based on the filter similarities of the asteroid colors to K0 to K2V stars. The first more complete asteroid taxonomy was based on a synthesis of polarimetry, radiometry, and spectrophotometry, using a survey of 110 asteroids [1]. The defined a class *C* for dark carbonaceous objects, a class with the label *S* for siliceous objects, and *U* for objects that did not fit either class. This system has the disadvantage that it was not detailed enough and is based on the exclusion principle. The groundwork for the most complete taxonomy, that significantly expands the previous taxonomy has been proposed by Tholen [16]. This taxonomy is, with small modifications, still in use today. Tholen established several asteroid classes, which are based on the albedo as well as eight channel color indices. The overall albedo, as well as the spread and inclination of the color values, distinguishes the classes. Tholen based his taxonomy on the cluster analysis of a normalized set of the color and albedo indices. The aim of asteroid taxonomy is to link those classes to heliocentric distance, diameter, and rotation rate, but also to the evolution, creation and dynamic (orbit-attitude) long term behavior of asteroids. Relatively independently a second asteroid classification has been induced recently. These second classification is a risk assessment of asteroids, with respect of their miss-distance to the Earth.

A second increasingly relevant task of an asteroid taxonomy is the quantification of the impact risk. The impact risk according to the so-called Palermo scale [2]

is based on the expected energy of in impact, normalized with the background risk and the time frame of the collision. The energy of the impact is correlated to the mass and the impact velocity. The impact mass is traced back to the albedo and density (material properties) of the object and hence correlates to the Tholen albedo-color taxonomy. This is also a hint that the spectral classes correspond to a physical reality.

In the case of artificial objects, a historically new situation arises. For the first time the ancestral state is theoretically and a priori fully known as the objects originate from known man-made objects and materials. This is a state that is normally determined at the end of the development of a taxonomy. However, it does not eliminate the task of identification as derived from the data that is collected with the means at hand. Hence, in this case the taxonomy is done in reverse as compared to other applications in science or other disciplines. The question is, how does the physical reality influence the observed dynamical state the objects are in, nominal orbital state, as well as quantities that are of interest of us, such as the potential hazard those objects bear for the preservation of space environment.

The topic of finding a taxonomic system for artificial space objects is relatively young [18, 5]. Wilkins suggests to make use a Linean system, dividing the space objects in kingdoms, geni, families, orders, classes, lhyla and kingdoms. The Linean system is historically based on similarity criteria and obvious physical traits. In modern biology, with the rise of Darwins biological system and even more nowadays with modern genetics, the Linean system has been replaced by the Phylogenetic system. In the Phylogenetic system, an ancestral tree is build, each node in the tree defines a split in the common ancestor. A similar first approach to this has been made in [5], but is missing the rigorousness that is required for the task.

In the current paper a rigorous development of a Phylogenetic system of space objects is been made in a first step, defining the framework and analogies of the system, which allows to trace back all object to their origin of creation in principle. This is the so-called a priori step. This is followed by two empirical steps: I the first step, the connection of the a priori classes and the probability of detection is shown. In the second step, a reduction on the physical characteristic of the orbit is pursued. In a weighted minimal tree approach a grouping of the known space objects is done, in order to draw the analogy to the a priori taxonomic system. In a last step a hazard value is established based to establish a measure for the passive hazard a number for the groups of space objects according the risk they pose for crossing space objects.

Table 1. Key Physical Characteristics serving as the "genetics" of the taxonomy. The orbital regime itself serves as a third dimension to the whole scheme.

trait	a priori established discriminators
orbit	controlled (C) – uncontrolled(U)
attitude	controlled stable (S) – regularly spinning/rotating (R)– tumbling/irregular(T)
materials	composite of many materials (M)– few materials (F)– single material (S)
shape	regular convex (X) – regular (with concavities) (R)– irregular (I)
size	large (> 1.5m) (L)– medium (M) – small (< 10cm) (S)
AMR	HAMR(> 2m ² /kg) (hi)– medium AMR (me)– low AMR (< 0.8m ² /kg)(lo)

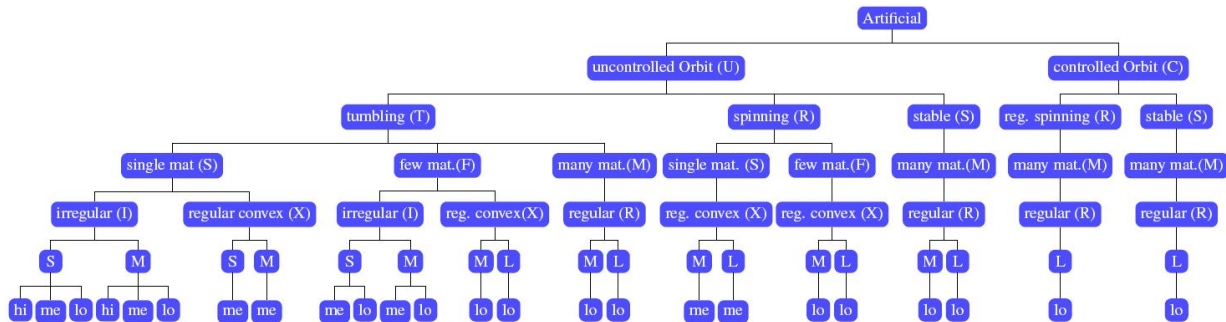


Figure 1. Classes based on key characteristics.

Table 2. Classes based on the physical characteristics combination.

name	Example member
operational	
CRMRLlo	spin stabilized maneuvering satellite
CSMRLlo	stabilized maneuvering satellite
USMRLlo	stabilized satellite
USMRMlo	stabilized (multi) cubesat
passively operational/debris - mission related/decommissioned intact	
URFXLlo	upper stages/ cal spheres /decommissioned satellites with initial spin
URFXMlo	smaller upper stages/ cal spheres with initial spin
URSXLme	e.g. covers or other mission related objects with initial spin
URSXMme	smaller covers or other mission related objects with initial spin
Debris-decommissioned/mission related intact	
UTMRLlo	decommissioned satellites
UTMRMlo	decommissioned (multi)cubesats
UTFXLlo	tumbling upper stages
UTFXMlo	tumbling smaller mission related objects (bolts)
UTSXLme	tumbling mission related objects (covers)
UTSXMme	tumbling mission related objects (covers)
Debris-fragments, explosion pieces, delamination remnants	
UTFIMlo	medium sized composite compact piece
UTFIMme	medium sized composite large area piece
UTFISlo	small sized composite compact piece
UTFISme	small sized composite large area piece
UTSIMlo	medium sized single material compact piece
UTSIMme	medium sized single material large area piece
UTSIMhi	medium sized single material large area piece
UTSISlo	small sized single material compact piece
UTSISme	small sized single material large area piece
UTSIShi	small sized single material very large area piece

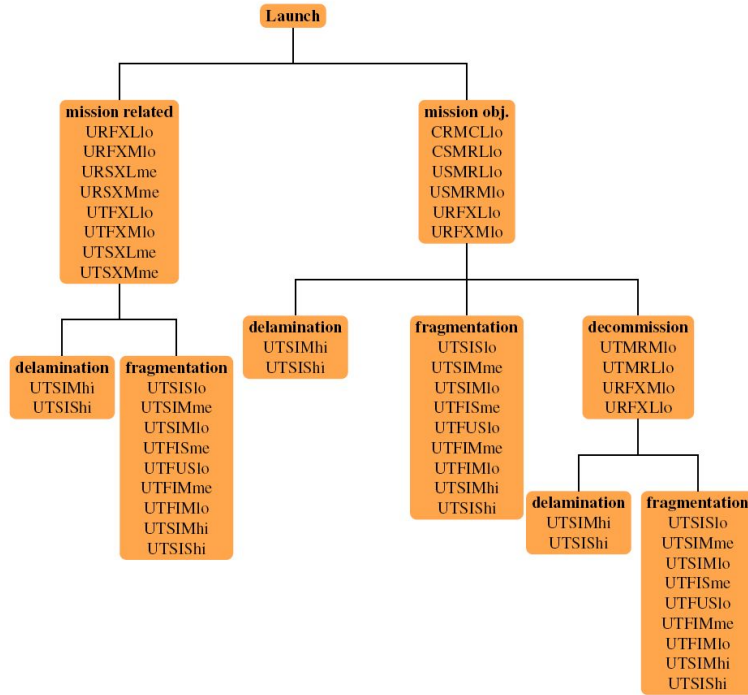


Figure 2. Association of the classes with the class transition processes.

2. KEY PHYSICAL CHARACTERISTICS CLASSIFICATION

If we want to adopt a Phylogenetic system for space objects, it has to be clear, which our analog to the genetics is. Of course we are only based on the physical characteristics of the objects. Inspired by the characteristics Tholen was investigating, the following five characteristics have been established: Orbit (state, region), Attitude state, materials, shape, size, area-to-mass ratio (AMR). The AMR is more a replacement of the weight of the body, which is not directly accessible via the measurements, but is readily determined from the AMR if size information is available. The orbit includes the orbital state, especially if it is a controlled or uncontrolled orbit. However, as we will see later, the distinction between orbital regions is like a third dimension to the tree, which is in itself beyond orbital limitations, but could be build also in each orbital region separately, with different numbers of inhabitants in the different categories. The attitude state is the characteristic how the attitude of the object is evolving over time, is it actively stabilized, naturally stable, spinning moderately around one axis, spinning in irregular manner. The material parameter describes the materials of the object, it is a single material, a few or a composite of many different materials. The materials parameter does include inner and outer materials of the object. Although inner materials are not observable, they can become relevant in a collision. The shape parameters is describing the shape of the object, in general one has to distinguish between a well defined shape which can possibly be

known a priori and a irregular shape, as it is the result in collisions. The size is distinguished in three different kinds, small, which is below 10cm, medium, which is between 10cm and 1.5 meter and larger than 1.5 meter in diameter. The threshold values are oriented towards below cube sat size, cubesat size made of multiple cubes, and sizes of smaller mission related objects, and large objects, which are whole satellites. The AMR value splits in three categories, HAMR, which AMR values larger than 2, medium AMR, between 0.8 and 2, and low AMR below $0.8 \text{ m}^2/\text{kg}$. An overview can be found in Tab. 1. The characters in paranthesis are used to define the characteristics of the categories that are formed.

Theoretically, evaluating all permutations of the characteristics, 468 classes would have to be formed. Fortunately, not all of them are populated, and the majority of classes can be excluded from the start. Fig.2 shows the explication of the permutations that are realized. The order at which the tree is split is not relevant. It follows the intuitive order that is listed in Tab.1. Classes are excluded by the following criteria. Objects that are both orbit and attitude controlled require a full satellite, which consists of many materials and must be larger than cube sat size. Those objects, necessarily have a low AMR value. High and medium AMR values, can only be achieved using few or single materials. Fragmentation pieces are the smallest artificial space objects, they have also necessarily an irregular shape, and can have all kinds of AMR values. Tab.2 list all 24 classes that have been found and lists objects that are in these classes as examples.

Table 3. Processes inducing class associations and class changes.

1	launch
2	decommission/system failure
3	fragmentation (collision, explosion, break-up)
4	delamination
5	reentry

These classes are build from the combination of physical characteristics or key aspects. With this background we are now able to fit those classes in the known creation processes. The known creation processes that place objects in their initial class but are also responsible for them to change their class are the following: launch, decommission/system failure, fragmentation (explosion, collision), delamination, breakup, reentry. We neglect reentry here, as this leads to the destruction of the object, and hence no classification is needed any more. Taking processes as the Kessler Syndrome, all objects have the tendency to converge to classes that are listed under the UTFI_ and UTSI_ classes. They are also the ones that are underrepresented in the official catalog, as they are small sized and hard to detect. The methods that induce class changes are listed in Tab.3. In Fig.2 one can see the classes that are listed together with the processes of class changes. The figure clearly shows, that the classes are on different hierarchical levels. Some equal to the status the object have directly after the launch, others underwent further changes, and have transitioned between classes to their current class.

3. DERIVATIONS FROM THE CLASSIFICATION

3.1. Connection with the Probability of Detection

The probability of detection is directly linked to the physical properties and hence to the classes that are laid out. For the overall probability of detection P_i of a class of objects i , three things have to be taken into account. The probability of detection of the class in itself, based on its physical key properties P_{phys} , that define the class, the observation scenario and sensor characteristics that is used P_{sensor} , and the interclass probability $P_{rel.}$. The latter states the amount of objects, that are in the certain classes, that are theoretically detectable by the specific sensor. Taking only the latter probability into account necessarily leads to wrong results, e.g. when used as input in a Bayesian filtering[18]. The probability of detection for a specific class is hence defined as:

$$P_i = P_{phys,i} \cdot P_{sensor} \cdot P_{rel.,i} \quad (1)$$

This is especially important when we imagine, considering the probability of detection for small fragments, of the classes UTSIS_ and UTFIS_ . The majority of the

objects can be found in that class. But, they are in the majority of cases beyond the detection limit of the sensor, hence have a very low probability of detection overall. For the classification in a filter setup, one might consider to renormalize the probability expression, so all possible classes add up to probability of one again:

$$\bar{P}_i = \frac{P_{phys,i} \cdot P_{sensor} \cdot P_{rel.,i}}{\sum_{i=1}^{24} P_i} \quad (2)$$

$P_{rel.,i}$ is highly dependent on the specific model that is used, e.g. does one focus on the publicly available space object catalog, or on in situ measurements, or on data from independent sensor networks, such as ISON. The evaluation of this quantity is subject to a separate paper. Here, we will focus on the evaluation of the first part.

For optical sensors, the detection probability is determined via the signal to noise ratio (SNR). For a detailed assessment of the signal to noise ratio background sources, detector capabilities, atmospheric conditions and visibility constraints have to be taken into account [7]. For the connection to taxonomy, we choose a simplified approach. The signal to noise ratio can be approximated, when we only take the object signal itself into account:

$$S/N = \frac{S}{\sqrt{S}} = \sqrt{S} \quad (3)$$

The signal has two parts, the detector dependent part, and the object dependent part. The signal can be expressed as the following, averaging over the input spectra [7]:

$$\bar{S} = const. \cdot C_{sensor} \cdot C_{obsscenario} \cdot I_{object} \quad (4)$$

$$const = \frac{\pi}{4} \frac{\bar{\lambda}}{hc} \Delta \lambda I_{\odot} = 1.9457 \cdot 10^5 \quad (5)$$

$$C_{sensor} = (D - d)QE(\bar{\lambda}) \quad (6)$$

$$C_{obsscenario} = F \cdot \frac{e^{\tau(\bar{\lambda}) \sec(\pi - \epsilon_{ele})}}{p} \Delta t \quad (7)$$

$$I_{object} \cdot C_{sensloc} = A \cdot \Psi \cdot \frac{1}{x_{topo}^2} \quad (8)$$

$$(9)$$

The signal can be divided into four parts. A constant part $const$, a sensor part C_{sensor} and a object part, which is coupled with the sensor location part $I_{object} \cdot C_{sensloc}$. D is the sensor aperture, d the amount of the aperture which is obstructed. D is the aperture of the measurement device, d is the area of the aperture which is blocked by the construction e.g. of secondary reflection mirrors, I is the intensity of the source, that is measured, QE is the quantum efficiency of the detector, the exponential function accounts for the atmospheric extinction, τ is the wavelength dependent extinction coefficient. Here a zenith angle dependent wavelength dependent attenuation is assume, c is the speed of light and h is Planck's constant, and Δt is the integration time, and p is the number of pixels over which the signal is spread. F is the visibility condition, which evaluates, if the object is in

the field of view, above horizon, and not in Earth shadow. The function Ψ is the reflection function, it depends on both the sun-object-observer geometry and on the object properties. Ideally, we would like to decouple the object and the sensor location part, as our classification categories only depend on the object itself. However, as we will see below, this is not possible. Tab.4 lists the classes that have a different probability of detection. The underscores indicate a placeholder, all possible values in that part, cannot be discriminated from each other using the probability of detection. In the first part of the table, the S/R for the different classes are listed. In the second part of the table a standardized S/R for standard object of one meter size. This allows to multiply the S/R just with the appropriate object size in case it is given to a higher accuracy than just the limits of a specific class. We are deriving now averaged expressions for each of the pool of classes that are listed in the second part of Tab.4.

For a flat plate $I_{object} \cdot C_{sensloc}$ will take the following form [7]:

$$I_{object} \cdot C_{sensloc} = \frac{A}{x_{topo}^2} \cdot \cos \beta \frac{C_d}{\pi} \cos \gamma, \quad (10)$$

$\delta = \arccos \left(\frac{\vec{O} + \vec{S}}{|\vec{O} + \vec{S}|} \cdot \vec{N} \right)$, whereas \vec{O} is the direction of the observer, \vec{S} is the direction to the Sun, and \vec{N} is the normal vector. The dimension of the sun has been taken into account, where a_{\odot} is the radius of the Sun, and x_{\odot} is the distance from the object to the Sun. C_s, C_d are the diffuse and specular reflection components. No limb darkening effects have been accounted for. For a spherical object, the function reads as:

$$I_{object} \cdot C_{sensloc} = \frac{A}{x_{topo}^2} \frac{C_d}{\pi} (\sin(\alpha) + (\pi - \alpha) \cos \alpha), \quad (12)$$

where the function is scaled with the diffuse reflection coefficient C_d . α is the phase angle between the direction and the direction of the observer.

$_{S}R_{}$ which can come in the size medium to large, are actively stabilized. Their reflection can be assumed to be dominated by the solar panels, which are flat surfaces, which keep the same angle to the sun, zero or close to zero angle between the surface normal vectors and the vector to the sun. This simplifies Eq. 10 to:

$$\langle I_{object} \cdot C_{sensloc} \rangle_{S}R_{} = \quad (13)$$

$$\frac{A}{x_{topo}^2} \cdot \cos \beta \frac{C_d}{\pi} + \frac{\tau \cdot C_s \cdot x_{\odot}^2}{a_{\odot}^2}, \quad (14)$$

which then equals a simple $\cos \beta$ phase angle dependence. For $_{R}R_{}$ and $_{R}R_{}$ a high symmetry of the object can be assumed. Most of the times, the objects in this class have some kind of cylindrical or half-round shape. For simplicity as we do not know the exact orientation of the cylinder we assume, it can be approximated

with a spherical surface, exposing most light from some kind of round surface as the cylinder cover, and/or half round upper and lower parts of the cylinder. We also assume, as the object is stabilized in some sense, the rotation axis is nearly perpendicular to the line of sight. The two classes are discriminated by their shape, that is do concavities occur or not. Früh et al [6] showed, that self-shadowing can be approximated by assigning different shadow probability values which can be used to scale the reflectivity. For $_{R}X_{}$ no self shadowing occurs, it can be approximated with Eq.13. For $_{R}R_{}$ a diminishing factor has to be calculated.

$$\langle I_{object} \cdot C_{sensloc} \rangle_{R}X_{} = r \cdot \langle I_{object} \cdot C_{sensloc} \rangle_{R}R_{}, \quad (15)$$

where r is the self-shadowing probability coefficient. it can reach values of zero, total self-shadowing to 1, no self-shadowing. For a given surface r is calculated as[6]:

$$r = \frac{1}{2\pi} (\arccos(e_1 \cdot e_2) + \arccos(e_3 \cdot e_4)), \quad (16)$$

where e_{1234} are the unit vectors connecting the position of the sub-facet midpoint with the edges of the concave plane. See Früh et al [6] for further details. In the absence of the concrete shape of the object, an exact value for r cannot be readily determined. The concrete value depends on how many surfaces have a convex relation. For members of the $_{R}R_{}$ group, only small concavities are expected, self-shadowing may be caused by antenna, or small concavities only, hence a small value of nearly one, 0.9 is assumed for r .

The classes $_{T}R_{}$, $_{T}X_{}$, $_{T}I_{}$ all deal with freely tumbling objects with different shape properties. Schildknecht [14] showed, that uniformly tumbling diffuse reflective flat plates, maybe be approximated by a sphere with a diminished radius (factor 1/3), however, the integration assumes, that all angles are swept uniformly. Simulations of objects have shown that this is not the case [8, 6]. Angles that are not swept are like self-shadowed concavities, which do not reflect any light in the direction of the observer. This leads to the following equations:

$$\langle I_{object} \cdot C_{sensloc} \rangle_{T}R_{} = \quad (17)$$

$$\frac{A}{3 \cdot x_{topo}^2} \cdot \frac{C_d}{\pi} (\sin(\alpha) + (\pi - \alpha) \cos \alpha) \cdot q$$

$$\langle I_{object} \cdot C_{sensloc} \rangle_{T}X_{} = \quad (18)$$

$$\langle I_{object} \cdot C_{sensloc} \rangle_{T}R_{} \cdot r'$$

$$\langle I_{object} \cdot C_{sensloc} \rangle_{T}I_{} = \quad (19)$$

$$\langle I_{object} \cdot C_{sensloc} \rangle_{T}R_{} \cdot r''$$

where q is the factor that accounts for the non-regular tumbling, and r' and r'' are the factors accounting for the self-shadowing in the regular shape with concavities and irregular shape. A value of $q = 0.8$ is taken into account, which is consistent with the simulations in [8], r' has a value of 0.7, and r'' of 0.6, as more self-shadowing is expected for irregular random shapes. Putting it back

Table 4. Probability of Detection and S/R.

name	S/R standardized	factors for non-standardized versions
_S_RL_	49.8	$\sqrt{C_{sensor}C_{obsscenario} \cdot 10^6 \cdot x_{topo}^{-2} \cos \beta}$
_S_RM_	25.7	$\sqrt{C_{sensor}C_{obsscenario} \cdot 10^6 \cdot x_{topo}^{-2} \cos \beta}$
_R_XL_	49.8	$\sqrt{C_{sensor}C_{obsscenario} \cdot 10^6 x_{topo}^{-2} (\sin(\alpha) + (\pi - \alpha) \cos \alpha)}$
_R_XM_	25.7	$\sqrt{C_{sensor}C_{obsscenario} \cdot 10^6 x_{topo}^{-2} (\sin(\alpha) + (\pi - \alpha) \cos \alpha)}$
_R_RL_	44.8	$\sqrt{C_{sensor}C_{obsscenario} \cdot 10^6 x_{topo}^{-2} (\sin(\alpha) + (\pi - \alpha) \cos \alpha)}$
_T_RL_	44.5	$\sqrt{C_{sensor}C_{obsscenario} \cdot 10^6 x_{topo}^{-2} (\sin(\alpha) + (\pi - \alpha) \cos \alpha)}$
_T_RM_	23.0	$\sqrt{C_{sensor}C_{obsscenario} \cdot 10^6 x_{topo}^{-2} (\sin(\alpha) + (\pi - \alpha) \cos \alpha)}$
_T_XL_	37.2	$\sqrt{C_{sensor}C_{obsscenario} \cdot 10^6 x_{topo}^{-2} (\sin(\alpha) + (\pi - \alpha) \cos \alpha)}$
_T_XM_	19.2	$\sqrt{C_{sensor}C_{obsscenario} \cdot 10^6 x_{topo}^{-2} (\sin(\alpha) + (\pi - \alpha) \cos \alpha)}$
_T_IM_	17.8	$\sqrt{C_{sensor}C_{obsscenario} \cdot 10^6 x_{topo}^{-2} (\sin(\alpha) + (\pi - \alpha) \cos \alpha)}$
_T_IS_	4.45	$\sqrt{C_{sensor}C_{obsscenario} \cdot 10^6 x_{topo}^{-2} (\sin(\alpha) + (\pi - \alpha) \cos \alpha)}$
_S_R_	28.7	$\sqrt{A \cdot C_{sensor}C_{obsscenario} \cdot 10^6 \cdot x_{topo}^{-2} \cos \beta}$
_R_X_	28.7	$\sqrt{A \cdot C_{sensor}C_{obsscenario} \cdot 10^6 x_{topo}^{-2} (\sin(\alpha) + (\pi - \alpha) \cos \alpha)}$
_R_R_	27.6	$\sqrt{A \cdot C_{sensor}C_{obsscenario} \cdot 10^6 x_{topo}^{-2} (\sin(\alpha) + (\pi - \alpha) \cos \alpha)}$
_T_R_	27.3	$\sqrt{A \cdot C_{sensor}C_{obsscenario} \cdot 10^6 x_{topo}^{-2} (\sin(\alpha) + (\pi - \alpha) \cos \alpha)}$
_T_X_	21.5	$\sqrt{A \cdot C_{sensor}C_{obsscenario} \cdot 10^6 x_{topo}^{-2} (\sin(\alpha) + (\pi - \alpha) \cos \alpha)}$
_T_I_	19.9	$\sqrt{A \cdot C_{sensor}C_{obsscenario} \cdot 10^6 x_{topo}^{-2} (\sin(\alpha) + (\pi - \alpha) \cos \alpha)}$

together, Tab.4 shows the signal to noise ratios. The first entry is for a standardized setup. A phase angle of zero is assumed, a standard distance of 10 000 km, a one meter aperture with $d = 0$, a quantum efficiency of 1.0 and visibility constraints are neglected $F = 1$. For the mean wavelength a value of 600nm has been assumed. For the second part of the table, where the discrimination in size classes has been neglected, an area of 1 has been assumed. For the sizes, 3m, 0.8m and 0.05 meters has been used. This just allows to multiply all quantities to the standard value in case they are shifted.

3.2. A Hazard Scale

A second application of the classes is the hazard scale. A hazard scale is similar to the Palermo scale in asteroid physics. In general the severity of a collision is linked to the energy and impulse conservation of the participants involved in a possible collision process. That is the mass of the objects involved, material properties, and their relative velocities.

A hazard scale can be defined. As before in the connection to the it is only concerned with a subset of the physical keys that are established in the taxonomy. However, of course. Those are the size and the AMR only, and possibly if the object is in an controlled orbit or not, which would allow for possible collision avoidance or not. Attitude, material and shape however, are relevant when it comes to the accuracy of the predicted orbits, which eventually allow for collision avoidance measures. A hazard value h can be defined via the energies that are involved:

$$h = \frac{1}{2} \frac{s}{AMR} \cdot v^2 = C_{class} \cdot C_{orbit} \quad (20)$$

s is the size of the object, and v its velocity. The velocity of course depends on the orbit the object it in. The velocity is approximated as the arithmetic mean of the apogee and perigee velocity, leading to the following equation:

$$C_{orbit} = \left[a \cdot n \cdot \frac{1 + e^2}{(1 - e)(1 + e)} \right]^2 \quad (21)$$

where a is the semi-major axis, n the mean velocity and e the eccentricity. This leads to the following hazard values as displayed in Tab.5. For the AMR values, the values of $4m^2/kg$, $1.4m^2/kg$ and $0.4m^2/kg$ has been used, for the sizes, 3m, 0.8m and 0.05 meters. For the orbit a mean velocity of 1 km/s has been used to scale the values.

3.3. Clustering of Orbital Space Level

The orbital space same as the creation, is a level to the taxonomy. Different classes appear at different levels only, some may appear in all levels. A cluster analysis

groups data by means of a similarity criterion in a selected feature space. The cluster analysis allows the determination of interrelationships within sample data. In general, one distinguishes between hierarchical clustering, heuristic segmentation methods and partitioning methods involving objective functions. Whereas the latter two methods produce clustered data on the same level, hierarchical clustering methods arrange data in nested sequences of groups, and can be displayed in a dendrogram, or tree structure.

Cluster analyses have a long tradition in taxonomy of natural objects. In biological taxonomy of bacteria, minimum distance sorting in a equal weighted feature space has been determined to lead to a classification [15]. A similar approach has been applied to a small set of asteroid spectra [3]. Tholen has used minimal spanning trees to establish an asteroid taxonomy [16]. The results of Tholen were confirmed using the same data and artificial neural network clustering [10]. Zahn compared different nearest neighbor algorithms to the minimal tree structure for clustering, proving the efficiency for cluster detection and pattern recognition, especially for irregular patterns [19]. Extensive research has been done on minimum spanning Euclidean trees, where the distance in a Euclidean parameter space is used as the measure of similarity [9, 12]. A greedy algorithm for finding a minimal tree is also being used [13], but comes with a large computational burden. In two dimensions, Delaunay triangulation provides a mean to supplement Prim's algorithm [4], though this is not feasible for higher dimensions. In this paper the focus is on hierarchical methods for clustering. Furthermore it is assumed that the number of clusters is not a priori known, and that a priori means have been defined.

The sheer amount of space resident objects, even when only cataloged objects are taken into account is very large, which makes the direct application of a minimal tree for clustering not very attractive. A modification of the Iterative Reducing and Clustering Using Hierarchies (BIRCH) algorithm is applied [20]. BIRCH is a very effective algorithm, leading to a hierarchical clustering in a single run. However, only the first step is used, ordering the data in a so-called CF (Cluster Feature) tree. A primary CF tree is created in a single run. The classical BIRCH algorithm then continues by slimming down the tree, with different resorting and merging techniques used to overcome some of the shortcomings of the initial CF tree. In the work presented here, a minimal tree is implemented as a second step, deviating from other CF combined approaches. Cluster features are a triple, consisting of the number of data points, which have been merged in the cluster, the linear and quadratic sum of the data points. This allows for a convenient adding of new data points into existing clusters. In the current approach the last entry is substituted by the sum of the radar cross sections (RCS). The feature consists of the three following entries:

$$CF = (N, \sum \vec{x}_i, \sum RCS_i), \quad (22)$$

Table 5. Taxonomy based hazard values.

name	h standardized [J]	factor for non-standard [m/s]
C__Llo	C3.750	v^2
U__Llo	3.750	v^2
U__Mlo	1.000	v^2
U__Slo	0.063	v^2
U__Lme	1.071	v^2
U__Mme	0.288	v^2
U__Sme	0.018	v^2
U__Mhi	0.100	v^2
U__Shi	0.006	v^2

N is the number of objects in the cluster, \vec{x}_i is the five dimensional vector of to the object in normalized and cropped orbital element space, and RCS is the radar cross section of the single objects that have joined the cluster. The distance, which is used in determining the threshold, between two clusters or between an existing cluster and a new data point is determined as the following

$$d_{CF_1CF_2} = \sqrt{\left(\frac{\sum \vec{x}_{1i}}{N_1} - \frac{\sum \vec{x}_{2i}}{N_2}\right)^2}, \quad (23)$$

which makes direct use of the CF structure, which also makes it easy to join two clusters together, by simple vector addition. Two different algorithms have been implemented to group the elements. The first step is identical in both, a threshold T is determined on the leaf level for the maximum radius of a leaf-cluster. This means, these clusters have a circular structure. For both algorithms, a threshold value for the number of leafs that can be combined in one node, cannot be larger than a maximum number B , and similarly a maximum number of nodes in a root of L . This allows for deviations from the circular shape. Nodes and roots are split, when the maximum numbers are reached, sorting out the leaf or node, respectively, that is furthest from the mean, determined by the values stored in the node or root respectively. The difference between the algorithms is the following. In the classical BIRCH approach, the first node and root are filled until their threshold values are reached and then split according to the rule. This is computationally very efficient, one of the great advantages of the method. In the next step the next leaf is added to the node to which it is closest, and so on. In the real of a limited number of entries, this can lead to wrong results; the method relies on a *sufficient* amount of data points, that lead to enough splits in the nodes or roots, respectively, so no nodes and roots are kept, combining very diverse data points. *Sufficient* is determined by the amount of data in combination with the threshold values, but also depends on the diversity of the data, e.g. the number of outliers. That is the cost at which the computational savings are achieved. If the distribution would be perfectly uniform, the number of number_{leafs}/ B and number_{nodes}/ L are built. The number of data is nearly 20 000 objects, threshold values are chosen as low as 10 for

both roots and nodes. Nevertheless, the CF tree is cross checked with a different algorithm. In that algorithm, the leafs and on the next level the nodes are combined to the absolute closest node and root, respectively. Nodes and roots are split at the threshold values at the same criterion as in the BIRCH algorithm. The modified algorithm allows a larger number of nodes and roots that are built automatically when the data is very diverse, no limits on the size of the data that is analyzed is enforced. For a uniform distribution of leafs, a number of number_{leafs}/number_{closest_neighbours} is built, that is in a perfectly uniform distribution number_{closest_neighbours} is equal to two. If this number is larger than the threshold, this number is replaced by the threshold value and hence is equal to the BIRCH approach. To explain this further. BIRCH relies on the fact, that the nodes and roots are overpopulated in order to find meaningful nodes and roots, that represent the lower tree structures well, the alternative approach, does equal to BIRCH in the overpopulated case, but provides a more meaningful structure, in sparse regions, where overpopulation is not reached to enforce splitting in the BIRCH algorithm. It is hence more flexible to data which is not circularly shaped.

In a second step all leaf-nodes are taken as initial input data points in the minimal tree, with their centroid position as their new nominal position of a mean object. For those nodes, a minimal tree is fitted [13], which leads to the final clustering in cutting the longest links. Cutting the longest links sacrifices some of the hierarchical structure and leads to a flat clustering into same-level clouds.

For the analysis, two line elements (TLE) have been used as the source of orbital information. Radar cross sections from the satcat catalog have been used to supplement the data. In the case where no radar cross sections were available, a default value of 0.3 m^2 has been used. It is the very aim of the work to expand the classification to include light curve and spectral measurements, to supplement the orbital element classification. However, the present lack of light curves for the majority of objects made this intractable. A crucial point in even starting the clustering analysis is to express the quantities

in a comparable manner, which expresses the values common units and hence makes them comparable in the first place. The second step is to weight the different orbital elements in a physical meaningful way. To find a common scale, the semi-major axis is used as a scaling factor and eccentricity, inclination, right ascension of the ascending node (RAAN), and argument of perigee are expressed in units of lengths as well, for the specific orbit. Orbital anomalies are not included for the clustering analysis. For the scaling of RAAN and argument of perigee using the approximated value from the circumference of the ellipse u , independently of the specific anomaly, the system is assumed to be locally flat. Because the accepted distances are limited by the threshold T the locally flat approach is justified. The inclination i , RAAN Ω and argument of perigee ω are scaled as the following:

$$i', \omega', \Omega' = \frac{i, \omega, \Omega}{2\pi} \cdot u, \quad (24)$$

The circumference u is approximated by the following:

$$u = \pi(a + b) \left(1 + \frac{3\lambda^2}{10 + \sqrt{4 - 3\lambda^2}} \right) \quad (25)$$

$$\lambda = \frac{a - b}{a + b}, \quad b = \sqrt{a^2(1 - e^2)}, \quad (26)$$

where a is the semi-major axis. The eccentricity e is scaled to the linear eccentricity ϵ :

$$\epsilon = e \cdot a. \quad (27)$$

The absolute scales are necessary to determine the distance in the five dimensional space, so only the relative values enter the clustering process. One way to weight the orbital elements would be an equal weight for all elements. The topic of normalization cannot be overemphasized, since it directly determines and shapes the clustering, as it has the effect of *defining* what is regarded as dense region and close neighbors. The scaling and weighting is done a priori, to save computational time.

In the initial run for building the CF tree in the classical approach, a total number of 575 roots were found with a total number of 1206 nodes holding 5229 leafs, 1964 leafs hold more than one element. With the modified algorithm 599 roots were found, with a number of 1782 nodes. On the root level, the algorithms produce nearly the same roots, on the node level, a significantly larger amount of nodes are created with the modified approach. The orbital elements of the six cluster leafs with the largest amount of data points are listed in Tab.6. Those are all high inclination low Earth orbits with small eccentricities. The RCS sum of the clusters is of the order of eight to six meters. Similar orbital regions are covered by the roots containing the non-leaf nodes and leaf nodes. The orbital elements and radar cross section of the roots with the highest number of member objects created in the modified approach is displayed in Tab.7.

Table 6. Six most populated leafs in the circular cluster feature tree and their mid points: number of objects, semi-major axis (km), eccentricity, inclination (deg), argument of perigee (deg), RAAN (deg), radar cross section of the whole cluster (m)

# obj	a	e	i	ω	Ω	RCS
30	7177.6	0.009	98.72	85.73	40.57	9.00
29	7196.4	0.008	73.25	158.03	279.60	8.85
29	7152.8	0.004	74.04	145.01	286.79	8.70
27	7201.4	0.008	72.15	141.45	271.10	7.22
27	7144.8	0.004	74.04	143.10	299.69	8.10
26	7203.6	0.008	98.82	29.18	84.507	6.87

Table 7. Six most populated root nodes in the circular cluster feature tree and their mid points: number of objects, semi-major axis (km), eccentricity, inclination (deg), argument of perigee (deg), RAAN (deg), radar cross section of the whole cluster (m)

# obj	a	e	i	ω	Ω	RCS
197	7276.5	0.012	98.55	127.75	90.21	57.38
133	7546.6	0.056	77.07	81.70	97.40	83.75
131	7256.7	0.011	98.73	94.07	290.27	38.15
130	7361.2	0.010	97.16	73.26	341.12	41.81
129	7172.1	0.008	73.03	97.40	298.99	44.62

Fig.3 shows the inclination as a function of the semi-major axis and the eccentricity as a function of the right ascension of the ascending node for the leaf nodes determined in the pre-clustering step. In Fig.3(a) the densely populated area is clearly visible is between 7000 and 9000 km, which contains the leafs with the largest number of objects. The geosynchronous region around 42000 km is also clearly discernible. Fig.3(b) shows the accumulation of the objects at low eccentricities and around 0.7 for all right ascension values. The modified algorithm tends to provides a stronger focus on the densely populated areas and seems to captures better the overall structure, which is discernible in the data.

4. CONCLUSIONS

In this paper an initial taxonomy system for space objects has been established. The Taxonomy is based on the biological phylogenetic system. This lead to the definition of physical key features. Those features are orbital state, attitude, amount of different materials, shape, size and area-to-mass ratio. Each of the key features comes with different discriminators, at least two, at most three. All permutations of the discriminators would lead to a large number of classes. However, not all permutation have an object that corresponds to it in reality, which hence lead to the establishment of 24 object classes.

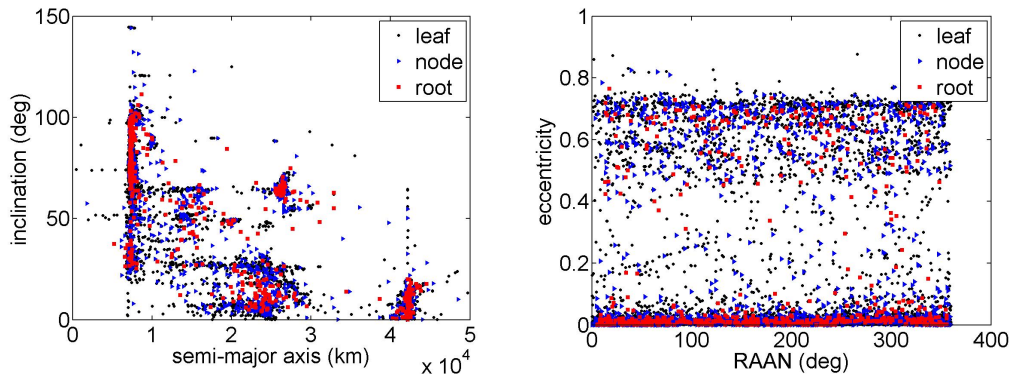


Figure 3. Cataloged space objects clustered in leaves, nodes and roots with the modified algorithm.

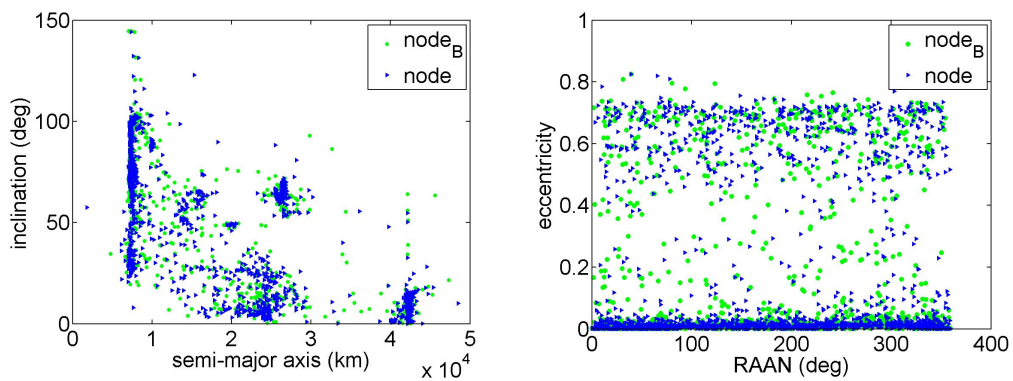


Figure 4. Leaves of clustered space objects with more than one member.

They classes are labeled defined by five capital letters, for the five first key features, and two lower case latter for the discriminators of the last category. If one does not want to distinguish between the discriminators of one specific feature and wants to include all, a lower space can replace the discriminator at that position.

Two levels to the taxonomy have been defined. Levels can hold one or more classes, classes can belong to more than one level. One level is the creation processes, another level the orbital region. For the clustering of orbital region a modified version of the BIRCH approach has been established. The densest orbital regions are in the sun-synchronous region. In total 599 roots were found, populated with 1782 nodes have been found.

The taxonomic classes and their combination with the orbit level allows to determine, averaged probabilities of detection using optical sensors for the different classes. Standardized values have been calculated, which can be multiplied with a factor that takes the concrete sensor and observation scenario into account. Similarly, hazard values for all classes have been defined, based on the kinetic energy of the different classes. The hazard values may be combined with the density of the orbital clusters that have been found.

ACKNOWLEDGMENTS

The first author would like to thank the National Science Foundation for providing the funding that supported this work.

REFERENCES

1. C.R. Chapman, D. Morrison, and B. Zellner. Surface properties of asteroids: A synthesis of polarimetry, radiometry, and spectrophotometry. *Icarus*, 25(1):104 – 130, 1975.
2. S.R. Chesley, P.W. Chodas, A. Milani, G.B. Valsecchi, and D.K. Yeomans. Quantifying the risk posed by potential Earth impacts. 159:423–432, 2002.
3. J.K. Davies, N. Eaton, S.F. Green, R.S. McCheyne, and A.J. Meadows. The classification of asteroids. *Vistas in Astronomy*, 26, Part 3(0):243 – 251, 1982.
4. C. Eldershaw and M. Hegland. Cluster analysis using triangulation. *Computational Techniques and Applications: CTAC97*, page 201208, 1997.
5. C. Früh. Development of an initial taxonomy and classification scheme for artificial space objects. In *Proceedings of the Sixth European Conference on Space Debris, ESOC, Darmstadt, Germany*, 2013.
6. C. Früh and M. Jah. Coupled orbit-attitude motion of high area-to-mass ratio (hamr) objects including self-shadowing. *Acta Astronautica*, submitted, 2013.
7. C. Früh and M.K. Jah. Detection Probability of Earth Orbiting Using Optical Sensors. In *Proceedings of the AAS/AIAA Astrodynamics Specialist Conference, Hilton Head, SC*, 2013.
8. C. Früh, T. Kelecyc, and M. Jah. Coupled orbit-attitude dynamics of high area-to-mass ratio (hamr) objects: Influence of solar radiation pressure, shadow paths and the visibility in light curves. *Celestial Mechanics and Dynamical Astronomy*, accepted, 2013.
9. O. Grygorash, Yan Zhou, and Z. Jorgensen. Minimum spanning tree based clustering algorithms. In *Tools with Artificial Intelligence, 2006. ICTAI '06. 18th IEEE International Conference on*, pages 73–81, 2006.
10. E. S. Howell, E. Mernyi, and L. A. Lebofsky. Classification of asteroid spectra using a neural network. *Journal of Geophysical Research: Planets (19912012)*, 99(E5):10847–10865, 1994.
11. E. Mayr. *Systematics and the Origin of Species*. Columbia University Press, 1942. ISBN: 9780674862500.
12. F. P. Preparata and M. I. Shamos. *Computational Geometry: An Introduction*. Springer-Verlag New York, Inc., 1985.
13. R. C. Prim. Shortest connection networks and some generalizations. *Bell System Technology Journal*, 36:1389–1401, 1957.
14. T. Schildknecht. *The Search for Space Debris Objects in High-Altitude Orbits*. Astronomical Institute, University of Bern, 2003. Habilitation treatise.
15. P. H. A. Sneath. The application of computers to taxonomy. *Journal of General Microbiology*, 17:201–226, 1957.
16. D. J. Tholen. Asteroid taxonomy from cluster analysis of photometry. The University of Arizona, 1984. PhD Thesis.
17. I. van Houten-Groeneveld and C. J. van Houten. Photometrics Studies of Asteroids. VII. *Astrophysical Journal*, vol. 127, 127:253, March 1958.
18. M. Wilkins. Towards an Artificial Space Object Taxonomy. In *AAS/AIAA Astrodynamics Specialist Conference, Hilton Head, SC*, 2013.
19. C.T. Zahn. Graph-theoretical methods for detecting and describing gestalt clusters. *Computers, IEEE Transactions on*, C-20(1):68–86, 1971.
20. Tian Zhang, Raghu Ramakrishnan, and Miron Livny. Birch: an efficient data clustering method for very large databases. *SIGMOD Rec.*, 25(2):103–114, 1996.